1 **Fast, multiplexable and highly efficient somatic gene deletions in adult mouse**

2 **skeletal muscle fibers using AAV-CRISPR/Cas9**

3

4 Marco Thürkauf[1], Shuo Lin[1], Filippo Oliveri[1], Dirk Grimm[2,3,4], Randall J. Platt[5,6] & Markus A. Rüegg[1*]

5

6 [1]Biozentrum, University of Basel, Basel, Switzerland

7 [2]Department of Infectious Diseases/Virology, Section Viral Vector Technologies, Medical Faculty,
8 Heidelberg University, Heidelberg, Germany

9 [3]BioQuant, University of Heidelberg, Heidelberg, Germany

10 [4]German Center for Infection Research (DZIF) and German Center for Cardiovascular Research (DZHK),
11 Heidelberg, Germany

12 [5]Department of Biosystems Science and Engineering (D-BSSE), ETH Zurich, Basel, Switzerland

13 [6]Department of Chemistry, University of Basel, Basel, Switzerland

14

15 Corresponding author: Markus A. Rüegg, markus-a.ruegg@unibas.ch

16   Abstract:

17   Molecular screens comparing different disease states to identify candidate genes rely on the

18   availability of fast, reliable and multiplexable systems to interrogate genes of interest. CRISPR/Cas9-

19   based reverse genetics is a promising method to eventually achieve this. However, such methods are

20   sorely lacking for multi-nucleated muscle fibers, since highly efficient nuclei editing is a requisite to

21   robustly inactive candidate genes. Here, we couple Cre-mediated skeletal muscle fiber-specific Cas9

22   expression with myotropic adeno-associated virus-mediated sgRNA delivery to establish a system for

23   highly effective somatic gene mutation in mice. Using well-characterized genes, we show that local or

24   systemic inactivation of these genes copy the phenotype of traditional gene-knockout mouse models.

25   Thus, this proof-of-principle study establishes a method to unravel the function of individual genes or

26   entire signaling pathways in adult skeletal muscle fibers without the cumbersome requirement of

27   generating knockout mice.

28   Introduction:

29   With the advent of –omics technologies that allow to correlate molecular signatures with specific

30   disease states of cells or tissues, there is an increasing need for methods to interrogate the function of

31   genes and pathways. Traditionally, forward and reverse genetics using targeted mutagenesis in

32   combination with transgenesis has been used. More recently, clustered regularly interspaced short

33   palindromic repeats (CRISPR)-mediated genome editing has become the method of choice for gene

34   engineering in many species and tissues (*1*).

35   When it comes to skeletal muscle tissue, studying gene function *in vivo* is particularly challenging.

36   Skeletal muscle is one of the largest organs constituting up to 50% of the mammalian body mass (*2*).

37   The size and the fact that muscle fibers, which are the functional contractile units of skeletal muscle,

38   form a syncytium with hundreds of myonuclei in a common cytosol, represent a substantial challenge

39   for somatic gene inactivation. Therefore, the method of choice for functional gene interrogation

40   studies in muscle remains transgenic mice generated *via* the Cre-loxP system. However, generation of

41   transgenic mice requires extensive breeding, making functional interrogation of multiple genes

42   cumbersome and time consuming.

43   Effective methods for somatic gene perturbation would offer huge advantages for screening

44   multiple muscle gene candidates. While RNA interference, which can silence a target gene by

45   introducing short hairpin (sh) RNAs (*3*), can acutely silence gene expression in muscle fibers (*4, 5*),

46   prolonged elimination of a gene product requires sustained, high expression of the shRNA. The

47   introduction of viruses, in particular adeno-associated viruses (AAV), as vehicles for delivering shRNAs,

48   opened the possibility of systemic administration (*6*). However, due to the lack of tissue-specific

49   control of shRNA expression, gene silencing occurs in all transduced cells. While next-generation AAV

50   capsids with designed tropism towards skeletal muscle tissue (*7-9*) may improve the off-tissue

51   targeting, all of them also target myocytes in the heart. Another challenge for somatic gene targeting

52   of muscle fibers is the overall heterogeneity of the tissue. Almost half of the nuclei in skeletal muscle

53   derive from non-fiber cells, such as muscle stem cells (MuSC), endothelial cells, fibro-adipogenic

54   precursors (FAPs), Schwann cells or tenocytes (*10*) and perturbation of their function often affects

55   muscle fibers as well. Therefore, for rapid functional gene interrogation in skeletal muscle fibers, an

56   efficient, multiplexable and muscle fiber-specific gene editing approach is sorely needed.

57   Here we establish a versatile tool for local and systemic skeletal muscle fiber-specific gene

58   knockout. This tool couples the advantages of CRISPR with newly developed, highly efficacious, AAV9-

59   derived viral capsids by using (i) mice engineered to constitutively or inducibly express Cas9 in skeletal

60   muscle fibers and (ii) delivering single guide (sg) RNAs with the myotropic AAVMYO (*7*). By targeting

61   key genes, we demonstrate that this system is capable of potently altering signaling pathways,

62   destroying neuromuscular junctions and stimulating muscle hypertrophy without needing to generate

63   germline gene-of-interest deletions.

64 Results:

65 **Constitutive expression of Cas9 in skeletal muscle fibers**

66 To express Cas9 at high levels in skeletal muscle fibers, we crossed Cre-dependent Rosa26$^{Cas9-EGFP}$

67 knockin mice (*11*) with mice expressing Cre recombinase constitutively (scheme in Fig. 1A) or upon

68 tamoxifen injection (scheme in Fig. S2A, S2B) in skeletal muscle fibers (*12, 13*). The resulting transgenic

69 mice were called Cas9mKI and iCas9mKI mice, respectively. Expression of Cas9 in Cas9mKI mice was

70 confirmed by immunohistochemistry for GFP (Fig. 1B). By Western blot analysis, Cas9 expression was

71 detected in all muscles tested but not in heart or liver (Fig. 1C). Most importantly, skeletal muscle mass

72 and function (Fig. 1D-I) as well as fiber-type composition and neuromuscular junction (NMJ) structure

73 (Fig. S1) of adult Cas9mKI mice were indistinguishable from control mice. Similarly, fourteen days after

74 tamoxifen injection, Cas9 was high in adult skeletal muscle but not detected in heart or liver of

75 iCas9mKI mice (Fig. S2). Together, these data confirm the strong and tissue-restricted expression of

76 Cas9 in skeletal muscle fibers of Cas9mKI and iCas9mKI mice.

77

78 **Robust *in vivo* gene editing using local AAV9-mediated sgRNA delivery into Cas9mKI mice**

79 To test whether high Cas9 expression would allow gene perturbation in skeletal muscle to an extent

80 required to lower protein levels, we selected *Prkca*, which codes for protein kinase Cα (PKCα). We

81 selected PKCα based on a combination of our experience characterizing PKCα as an mTORC2 target in

82 the brain (*14*), the availability of antibodies for Western blot analyses and because CRISPR has been

83 used to successfully eliminate PKCα in the retina (*15*). As low PKCα levels, due to loss of mTORC2, do

84 not affect skeletal muscle (*16*), we could determine the effectiveness of the system independent of

85 secondary effects by the loss of PKCα. Beside the published sgRNA (called sgPKCα-1), we tested initially

86 an additional sgRNA (sgPKCα-2) and included a non-targeting sgRNA (sgNT). Cultured C2C12 myoblasts

87 were transfected with a plasmid encoding the U6 promoter-driven sgRNA followed by an EFS

88 promoter-driven Cas9, the P2A self-cleavage peptide and puromycin N-acetyltransferase, which

89 confers puromycin resistance to transfected cells (Fig. S3A). After puromycin-selection, C2C12

90 myoblasts were differentiated into myotubes for five days. All selected cells expressed Cas9 and those

91 co-expressing sgPKCα-1 or sgPKCα-2, but not sgNT, showed strongly reduced levels of PKCα (Fig. S3B,

92 C). As sgPKCα-1 and sgPKCα-2 showed similar efficiency, we selected the published sgPKCα-1 (*15*) for

93 further characterization. To quantify the number of <u>in</u>sertions and <u>del</u>etions of bases (indels), we

94 sequenced genomic DNA in the region targeted by sgPKCα-1 and used the method of "<u>T</u>racking of

95 <u>In</u>dels by <u>De</u>composition" (TIDE). The total DNA-editing efficiency for sgPKCα-1 was 62.4 ± 1.6% (Fig.

96 S3D), with the majority of deletions lacking 1 base pair (-1 bp) followed by insertions of +1 bp (Fig. S3E).

97   Based on the high efficiency of sgPKCα-1 in editing *Prkca* and lowering the amount of PKCα in

98 cultured C2C12 cells, we next injected AAV9 expressing three copies of sgPKCα-1 and co-expressing

4

99 tdTomato under the CMV promoter (scheme in Fig. 2A) into *tibialis anterior* (TA) muscle of adult

100 Cas9mKI mice. Additionally, we co-injected neuraminidase, which has been shown to improve AAV9

101 transduction of skeletal muscle (*17, 18*). We used a non-targeting sgRNA (sgNT) as a control. Six weeks

102 after injection of either AAV9-sgNT or AAV9-sgPKCα-1 (3 x 10^{11} vg) into TA muscle of Cas9mKI mice,

103 several tissues were analyzed. Transduction efficiency was monitored by staining for tdTomato in TA

104 muscle cross-sections (Fig. 2B) and by measuring AAV genome copy numbers per nucleus in different

105 tissues (Fig. 2C). Expression of tdTomato was quite homogenous (Fig. 2B) and transduction rates

106 reached 99 ± 9.6 vg/nucleus in TA (Fig. 2C). Virus leakage into the blood stream resulted in strong liver

107 (117.8 ± 20.0 vg/nucleus) and weak heart (19 ± 3.3 vg/nucleus) transduction (Fig. 2C). To determine

108 genome editing efficiency, we again used TIDE in the targeted *Prkca* locus on DNA isolated from AAV9-

109 sgNT or AAV9-sgPKCα-1-transduced TA muscle (Fig. 2D). The background editing signal in AAV9-sgNT-

110 transduced muscle was 1.4 ± 0.5%, while the experimental muscle reached 20.3 ± 1.0% editing (Fig.

111 2D, E). As a consequence of CRISPR/Cas9-mediated DNA editing, PKCα protein was strongly diminished

112 in AAV9-sgPKCα-1-injected compared to AAV9-sgNT-injected TA muscle (Fig. 2F, G). The low amount

113 of PKCα still detected in AAV9-sgPKCα-1-transduced TA muscle may also derive from other muscle-

114 resident cells that express *Prkca* transcripts (*10*). Together, these data show that neuraminidase

115 treatment coupled with AAV9-mediated sgRNA delivery markedly reduced PKCα protein in the

116 targeted skeletal muscle of Cas9mKI mice.

117

Improved editing efficiency with AAVMYO for local sgRNA delivery into Cas9mKI mice

119 To further improve DNA editing and facilitate systemic applications (which is not possible when

120 injecting neuraminidase), we next tested a peptide-displaying AAV9 capsid variant, called AAVMYO,

121 with superior skeletal muscle fiber tropism (*7*). We compared the efficiency of AAVMYO-sgPKCα-1 with

122 AAV9-sgPKCα-1 by injecting 3 x 10^{11} vg of each, or a PBS control into TA muscle (Fig. 3A). Six weeks

123 post-injection, tdTomato expression was visibly higher in TA muscle as well as the nearby *extensor*

124 *digitorum longus* (EDL) and *gastrocnemius* (GAS) muscles of AAVMYO-injected mice than AAV9-

125 injected muscles (Fig. 3B). Cross sections from TA (Fig. 3B), EDL and GAS muscles (Fig. S4A) as well as

126 Western blot quantification from TA muscle (Fig. 3C-D) further confirmed higher tdTomato expression

127 in AAVMYO- than AAV9-injected muscles. Average transduction by AAVMYO, judged by AAV

128 genomes/nucleus, was at least 2.5 times higher than by AAV9 for all muscles, including the heart, while

129 transduction of the liver was markedly lower (Fig. S4B). The superior transduction efficiency of

130 AAVMYO over AAV9 upon intramuscular injection is in line with previous observations upon systemic

131 administration of AAVMYO and AAV9 (*7*). As a consequence of the more efficient transduction, the

132 amount of PKCα was also strongly diminished in AAVMYO-sgPKCα-1-transduced TA (Fig. 3C, D), EDL

133 (Fig. S4C, D) and GAS (Fig. S4F, G) muscles compared to AAV9-sgPKCα-1. TIDE analysis showed a higher

134   total editing efficiency of the sgPKCα-1-targeted locus by AAVMYO-sgPKCα-1 (22.4 ± 1.4%) than AAV9-

135   sgPKCα-1 (17.2 ± 0.9%) in TA muscle (Fig. 3E). Compared to the intramuscular injection of AAVMYO

136   into TA muscle, gene editing and knockdown efficiencies remained very similar in the adjacent EDL and

137   GAS muscles, while both values dropped with AAV9 (Fig. S4E, H).

138   To more precisely map genome editing frequency in the genomic DNA surrounding the sgPKCα-1

139   target site, we performed next-generation sequencing (NGS) of TA muscle DNA (Fig. 3F and Table S1).

140   The sum of all observed mutations with NGS was comparable to TIDE analysis; with average mutations

141   of 18.7 ± 0.6% for AAV9 and 23.1 ± 1.3% for AAVMYO (Fig. 3G). Independent of the AAV capsid variant,

142   the most frequent indels were short deletions (Fig. 3H). To test whether introduction of sgPKCα-1

143   caused off-target editing, we also sequenced the genome in the top four off-target sites as predicted

144   by the CRISPR-design tool CRISPOR (*19*). No significant sequence alterations were detected at these

145   loci (Fig. 3I).

146   Denervation and hence loss of muscle contraction has an immediate effect on gene expression in

147   myonuclei and results after a few days in exuberant muscle atrophy. It indirectly also affects satellite

148   cells and many other muscle-resident mononuclear cells. As somatic gene deletion may affect

149   innervation, we wanted to assess whether the gene editing system would also work during acute

150   denervation. To test this, we injected AAVMYO-sgPKCα-1 (3 x 10^{11} vg) or PBS (as a control) into TA

151   muscle of Cas9mKI mice before unilateral sciatic nerve transection 6 weeks later and then analyzed

152   muscle 14 days later. The denervation-induced loss of muscle mass was not different between PBS and

153   AAVMYO-sgPKCα-1-injected mice (Fig. S5A). Importantly, denervation did not affect the overall PKCα

154   knockdown efficiency or expression of the denervation marker HDAC4 (Fig. S5B, C). There was a slight

155   decrease in the total percentage of genome editing by sgPKCα-1 (Fig. S5D), which is likely due to the

156   increase in non-muscle fiber cells following denervation that do not express Cas9 (*20*). Together, our

157   data show that AAVMYO-mediated sgRNA delivery into TA muscle induces robust and specific *in vivo*

158   gene perturbation.

159

160   **AAVMYO supersedes AAV9 for systemic sgRNA delivery**

161   To evaluate efficiency for systemic gene editing, we next injected 1 x 10^{14} vg/kg of AAV9-sgPKCα-1 or

162   AAVMYO-sgPKCα-1 into the tail vein of 6-week-old Cas9mKI mice and collected tissues 6 weeks later

163   (scheme Fig. 4A). Expression of tdTomato was visually higher at autopsy and strikingly higher in cross-

164   sections of multiple muscles in mice injected with AAVMYO than with AAV9 (Fig. 4B). Similar results

165   were obtained for the heart (Fig. S6A). Numbers of viral genomes per nucleus were 4- to 6-fold higher

166   in limb muscles (TA, EDL, SOL and TRI) and more than 13-fold higher in the diaphragm (DIA) with

167   AAVMYO than AAV9 (Fig. 4C). In line with the high transduction efficiency, AAVMYO-sgPKCα-1 induced

168   2.2- to 7.6-fold higher DNA editing rates across different muscles than AAV9-sgPKCα-1 (Fig. 4D). The

169   most striking difference was seen in DIA muscle, where AAVMYO-sgPKCα-1 induced 19.1 ± 0.9% DNA

170   editing while AAV9-sgPKCα-1 induced only 2.5 ± 0.9%. Western blot analysis for tdTomato and PKCα

171   confirmed the superior systemic transduction of muscle tissue by AAVMYO-sgPKCα-1, with higher

172   tdTomato expression and stronger reduction in PKCα protein abundance than with AAV9-sgPKCα-1

173   (Fig. 4E-G).

174   We also tested systemic administration of additional capsid variants of AAVMYO, called AAVMYO2

175   and AAVMYO3, that were originally selected for their liver de-targeting qualities (*8*), which can be an

176   advantage for clinical applications. AAVMYO2 and AAVMYO3 were less efficient than AAVMYO, but

177   superior to AAV9, at transducing and therefore eliciting gene editing events in skeletal muscles (Fig.

178   S6) as well as heart muscle (Fig. S7A). Notably, both AAVMYO2 and AAVMYO3, showed strong liver de-

179   targeting (Fig. S7B-D). Nonetheless, because of the higher muscle tropism of AAVMYO, we opted to

180   use this variant in further studies.

181

182   **AAVMYO-CRISPR/Cas9-mediated knockdown recapitulates conditional knockout model phenotypes**

183   **for MuSK and myostatin/activin signaling**

184   After successfully demonstrating the effectiveness of our model to perturb gene expression within

185   skeletal muscle fibers, we asked whether we could recapitulate both loss and gain of muscle function

186   phenotypes by targeting genes known to play a fundamental role in the regulation of muscle structure

187   and growth.

188   We first chose to target the receptor tyrosine kinase MuSK, the signaling component of the

189   Lrp4/MuSK receptor complex for motor neuron-released agrin (*21*). MuSK is essential for the formation

190   and maintenance of the NMJ (*4, 22, 23*) and auto-antibodies against MuSK can cause myasthenia gravis

191   (*24*), a disease leading to NMJ loss. As AAVMYO transduces all skeletal muscle fibers with high

192   efficiency, we omitted tdTomato and instead focused on maximizing *Musk* gene editing, as no

193   functional sgRNAs have been described. To this end, we inserted seven different sgRNAs into the

194   constructs directed against exons localized in the 5' region of the *Musk* gene. In a first set of

195   experiments, we injected AAVMYO-7sgMusk (1.5 x 10^{13} vg/kg) or PBS (as a control) into the lateral tail

196   vein of Cas9mKI (scheme Fig. 5A). By following the body weight, we noted that AAVMYO-7sgMusk-

197   injected Cas9mKI started to lose weight after 14 days, reaching more than 20% at 20 days post injection

198   (Fig. 5B). Their all- and forelimb grip strength was significantly lower than in controls (Fig. 5C, D) and

199   they developed a severe kyphosis indicative of muscle weakness (Fig. 5E). Mice also showed signs of

200   muscle fibrillation and ataxia, suggestive of denervation. To confirm this hypothesis, we measured

201   mass in bulbar, fore- and hindlimb muscles. Indeed, all muscles of AAVMYO-7sgMusk-injected Cas9mKI

202   were severely atrophic compared to controls (Fig 5F). CRISPR/Cas9 editing in TA muscle resulted in an

203   almost complete loss of *Musk* mRNA expression (Fig. 5G). Whole-mount staining of the NMJ in the EDL

204 muscle confirmed the loss of MuSK, which resulted in the very strong reduction of acetylcholine

205 receptor (AChR) clusters (Fig. 5H). The presynaptic motor nerve terminals, visualized by a mixture of

206 the SV2, directed against synaptic vesicle glycoprotein 2A, and 2H3, directed against the

207 neurofilament-M protein, were still innervating the muscle fibers as in the controls (Fig. 5H). This loss

208 of postsynaptic structures upon MuSK depletion is consistent with the results of transgenic mice

209 deficient for Musk (*4, 22, 23*). Thus, our data show that the AAV-CRISPR/Cas9 system generates a

210 somatic gene knockout whose phenotype is identical to germline-based methods.

211 Next, we tested whether this system would also allow to restrict the depletion of MuSK to one or

212 a few muscles. This might be advantage as loss of genes that are essential for muscle function (such as

213 MuSK) will result in respiratory failure. As AAVMYO transduces the diaphragm well (see Fig. 4),

214 respiratory failure may jeopardize the in depth analysis of limb muscles. To do this, we injected

215 different doses of AAVMYO-7sgMusk into the right TA muscle of adult Cas9mKI mice (scheme Fig. 6A)

216 and monitored the mice for 5 weeks. As controls, we chose to inject either AAVMYO-7sgMusk into

217 wild-type (i.e. not expressing Cas9 in muscle) or injected PBS into Cas9mKI mice. As the two control

218 conditions did not differ, we pooled data for further analysis (Fig. 6B-H). Despite intramuscular

219 administration, mice receiving the highest dose of 3×10^{11} vg lost body mass (Fig. 6B) already 14 days

220 after injection, reaching 20% body mass loss at 21 days and therefore requiring a humane endpoint.

221 The second highest dose (1×10^{11} vg) induced measurable body mass losses by 28 days and reached

222 our euthanization threshold at 35 days, while the two lowest doses did not induce body mass loss (Fig.

223 6B). Analysis of hindlimb muscle mass in the injected leg showed a dose-dependent decline in mass,

224 which became significant compared to controls starting at a dose of 3.3×10^{10} vg (Fig. 6C). At the two

225 highest doses (3×10^{11} and 1×10^{11} vg), significant loss of muscle mass was also observed in all

226 contralateral, non-injected leg muscles compared to control mice (Fig. S8A). This highlights the high

227 efficiency of the system, as the low amount of AAVMYO circulating in the blood upon intramuscular

228 injection is sufficient to perturb gene function in remotely-positioned skeletal muscles (see also Fig.

229 S4). At the two highest doses, *Musk* expression was significantly reduced down to 3.1% and 6.3% of

230 control levels, respectively (Fig. 6D). *Musk* expression was also lower than in controls at a dose of 3.3

231 $\times 10^{10}$ and 1.1×10^{10} vg but both did not reach significance (Fig. 6D). As suggested by the overall loss of

232 body and muscle mass, *Musk* mRNA abundance was significantly lower in the diaphragm (Fig. S8B) and

233 the contralateral, non-injected TA muscle (Fig. S8C) compared to controls at the highest doses (8.9%

234 of control in the diaphragm; 10.7% of control in TA) but not at the two lower doses. These results

235 indicate that the lower dose of AAVMYO-7sgMusk largely restricts target knockdown to the injected

236 muscle. To test for functional consequences by the loss of Musk upon local AAVMYO-7sgMusk

237 injection, NMJ structure was examined in EDL muscle, which is adjacent to the TA muscle and hence

238 becomes sufficiently transduced by intramuscular TA injection. Consistent with the phenotype of

8

239   systemic MuSK depletion (Fig. 5H), postsynaptic AChR clusters were largely lost in AAVMYO-7sgMusk-

240   injected Cas9mKI mice compared to controls, irrespective of dose (Fig. 6E). As a consequence of the

241   loss of the postsynaptic structure, muscles become denervated, which causes re-expression of several

242   synaptic genes along the entire muscle fiber (*20, 25*). To quantify the extent of denervation, we

243   measured expression of mRNA coding for AChRα (*Chrna1*), the embryonic AChRγ subunit (*Chrng*) as

244   well as growth arrest and DNA damage-inducible 45a (*Gadd45a*). The abundance of all transcripts was

245   more than 10-times higher in the AAVMYO-7sgMusk-injected TA muscle of Cas9mKI mice than in

246   controls (Fig. 6F-H). Consistent with whole-mount NMJ staining, the fold-induction of denervation-

247   marker genes was independent of AAVMYO-7sgMusk dose. In summary, these experiments

248   demonstrate that the lowering the dose of the injected AAV allows to perturb gene function largely

249   restricted to the injected muscle without compromising the phenotype.

250   To test whether our system could also drive gain of muscle function, we next targeted myostatin

251   (GDF-8), a TGF-β family protein secreted by skeletal muscle that acts as an inhibitor of muscle size (*26*).

252   Deletion of *Mstn* in mice results in robust muscle hypertrophy (*27*) and naturally occurring *Mstn* null-

253   mutants cause hypermuscularity in many species, including cows and humans (*28, 29*). Myostatin

254   signals through a combination of type-2 and type-1 receptors. This signaling pathway is also activated

255   by several other ligands, including activin. The two ligand-binding receptors are activin A receptor type-

256   2/IIA (ACVR2A or ACTRIIA) and type-2/IIB (AAVR2B or ACTRIIB). The activin A type-2 receptors are

257   partially redundant as targeting both receptors elicits stronger muscle hypertrophy than deletion of

258   each receptor individually (*30*). Upon ligand-binding, the type-2 receptors form a complex with type-1

259   activin A receptor-like kinase-4 (ALK4) and ALK5, which are also partially redundant, to trigger

260   intracellular signaling.

261   To prevent partial compensation and to test the feasibility of the AAVMYO-CRISPR/Cas9 system

262   to delete several genes, we targeted both mouse *Acvr2a* and *Acvr2b* genes by simultaneously injecting

263   two AAVMYO viruses (each targeting one gene with seven different sgRNAs) at a dose of 3×10^{11} vg

264   (each virus) into TA muscle of 8-week-old Cas9mKI mice (Fig. 7A) and analyzed muscles 6 weeks later.

265   Virus-injected muscles expressed only 18% of *Acvr2a* and 26% or *Acvr2b* transcripts compared to PBS-

266   injected muscle (Fig. 7B), confirming successful targeting. During the 6 weeks, AAVMYO-sgAcvr2a/b-

267   injected mice gained significantly more body mass (Fig. 7C) and muscles of the injected leg were 40-

268   50% heavier than in PBS-injected mice (Fig. 7D), highly comparable to the phenotype of *Acvr2a/b*

269   double-knockout mice (*30*). Like in experiments targeting MuSK, the high dose intramuscular AAVMYO

270   spread systemically, causing similar gains in muscle mass in the contralateral leg as the injected leg

271   (Fig. S9A). Muscle growth in global *Mstn*-deficient mice is mediated *via* hyperplasia and hypertrophy

272   (*27*), while myostatin signaling blockade after weaning (> 3-4 weeks) predominately stimulates

273   hypertrophy (*26, 31, 32*). Consistent with these results, quantitative measurement of minimal fiber

274   feret diameter (*33*) using immunohistochemistry in TA muscles injected with AAVMYO-sgAcvr2a/b (Fig.

275   7E) showed a consistent rightward shift in fiber size distribution and a significant increase in mean fiber

276   size of all fiber types (Fig. 7F) without affecting fiber number (Fig. S9B). These results are highly

277   consistent with those obtained with knockout mice and demonstrate the utility of AAVMYO-

278   CRISPR/Cas9 to inactivate multiple genes and reproduce the phenotypes of traditional knockout mice,

279   without the need to breed additional mouse lines.

280   Discussion:

281   This article presents a rapid and highly efficient tool to investigate the function of single or multiple

282   genes in adult skeletal muscle fibers. Feasibility and efficiency of the system is demonstrated by

283   knocking out essential genes for the integrity of the NMJ and skeletal muscle fiber growth.

284   We show that high, long-term Cas9 expression in skeletal muscle fibers does not affect muscle

285   size or function. Others have used AAV to deliver Cre to LSL-Cas9KI mice to excise the stop cassette

286   and drive Cas9 expression (*11, 34*). While this approach allows for the use of Cas9-GFP as a transfection

287   marker and reduces any potential side effects of prolonged Cas9 expression, AAV-mediated delivery

288   of Cre would also lead to Cas9 expression in any AAV-targeted tissues, including the heart and liver. To

289   our best knowledge, highly specific AAV-compatible promoters for skeletal muscle fibers do not

290   currently exist. As such, our AAVMYO-CRISPR/Cas9mKI strategy represents a major advancement for

291   somatic gene perturbation of mouse skeletal muscle fibers.

292   While CRISPR/Cas9 systems for somatic gene deletion have been described for some tissues,

293   including brain and liver (*11, 35*), such a versatile tool has so far been missing for skeletal muscle fibers.

294   Previous work has demonstrated successful somatic gene editing using CRISPR in muscle stem cells

295   (MuSCs) although with rather low efficiency (*36, 37*). While editing efficiency can be increased by

296   sorting MuSCs based on a fluorescent transfection marker, this is not possible for multi-nucleated

297   skeletal muscle fibers. Thus, the successful depletion of a gene by CRISPR in muscle fibers is only

298   possible when indels are generated in both alleles in the majority of myonuclei. Such high efficiencies

299   are not required in CRISPR/Cas9-mediated editing approaches that aim to correct gene mutations

300   causing muscular dystrophies (*36, 38-42*). In these experiments, correcting the mutation in a subset of

301   myonuclei and in one allele is sufficient as the corrected protein will distribute in a large part of the

302   muscle fiber cytoplasm.

303   While CRISPR/Cas9-mediated gene deletion in mouse embryos has shortened the time to create

304   founder mice to a few weeks and created the possibility to target multiple genes simultaneously (*43*),

305   it still requires many founder breedings with different mouse lines to eventually achieve the final

306   genotype needed for a study. The method we established here allows to conditionally knock out a

307   single or multiple genes in muscle fibers without any prior breeding. We hypothesize that the use of

308   mice expressing Cas9 at high levels in all muscle fibers in combination with AAVMYO to deliver multiple

309   sgRNAs is key to achieve the efficient somatic gene deletions that mimic the phenotype of the

310   respective knockout mouse. Our method also allows for both, systemic or local (in a single muscle)

311   gene editing, which may be essential in cases where a gene knockout causes severe morbidity or death.

312   Thus, this method also contributes to the 3R principle by strongly reducing the number of mice needed

313   to investigate the function of genes *in vivo*.

314   The new method was established by targeting PKCα, as work in the retina has provided evidence

315   for an efficient knockout using CRISPR/Cas9 (*15*) and based on the availability of high-quality antibodies

316   to PKCα. Using this target, we were able to optimize the delivery method for the sgRNA by using

317   AAVMYO instead of AAV9. With this optimized set-up, the amount of PKCα was lowered by

318   approximately 80% in the injected muscle. Interestingly, DNA editing of the *Prkca* locus, measured by

319   TIDE analysis, did not reach 80% but was only 23%. Several reasons can account for the quantitative

320   difference between genome editing and loss of protein. First and foremost, only approximately 50%

321   of the nuclei in a muscle isolate are myonuclei (*44, 45*). The remaining nuclei are derived from mono-

322   nucleated cells, such as FAPs, macrophages, MuSCs, endothelial cells, smooth muscle cells or Schwann

323   cells. All these non-muscle fiber cells do not express Cas9 in the Cas9mKi mice and are hence not

324   edited. Hence, editing in muscle fibers would reach close to 50%. CRISPR/Cas9 editing in cultured

325   C2C12 myotubes using the same sgRNA resulted in 60% editing and a loss of the protein of more than

326   90%. With this in mind (60% editing measured by TIDE analysis results in the almost complete loss of

327   PKCα protein) and the fact that only 50% of the DNA in a muscle lysate are derived from myonuclei,

328   the real *in vivo* editing efficiency would likely be above 75%. Another possible contributor to the

329   incomplete editing efficiency may relate to the chromatin environment of the target site in the *Prkca*

330   locus (*46*), which may differ between cultured C2C12 cells and muscle fibers *in vivo*. Since PKCα protein

331   is mainly synthesized by muscle fibers (*10, 47*), the loss of the protein might be a better indicator for

332   the efficiency of gene deletion.

333   As a functional proof-of-concept, we also perturbed MuSK function, which is essential for NMJ

334   formation and maintenance (*21*). *Musk* expression in adult mice is confined to sub-synaptic nuclei,

335   which lay directly underneath the NMJ. Sub-synaptic *Musk* expression is based on local, NMJ-derived

336   signals that overwrite activity-mediated transcription suppression in non-synaptic myonuclei (*21*).

337   Denervation and hence loss of electrical activity results in *Musk* re-expression in non-synaptic

338   myonuclei. Hence, unlike *Prkca*, which is not specific to muscle fibers, efficient editing of myonuclear

339   DNA should be sufficient to abrogate *Musk* expression in whole-muscle lysates. Indeed, *Musk*

340   transcripts were reduced by 98% upon sgRNA expression. This strong reduction of *Musk* transcripts is

341   likely due to the use of multiple sgRNAs that edit the *Musk* gene at multiple sites, which, in turn, may

342   introduce large deletions that de-stabilize mRNA. Moreover, indels will result in frameshifts and the

343   occurrence of premature termination codons that cause nonsense-mediated mRNA decay. A strong

344   reduction of transcript levels was also observed for *Acvr2a* and *Acvr2b* using multiple sgRNAs.

345   Although the focus of our work was to use the MuSK knockdown as a proof-of-principle to

346   demonstrate efficiency of the method, our data also show that MuSK is essential for the maintenance

347   of the NMJ in the adult and that it is critical for muscle mass maintenance. This has so far only been

348   shown indirectly by (i) injection of the MuSK ectodomain into adult mice that triggered the production

12

349 of autoimmune antibodies and resulted in the deterioration of the NMJ reminiscent of myasthenia

350 gravis (*48*), (ii) local shRNA-mediated suppression of *Musk* by electroporation, which led to NMJ loss

351 (*4*) and (iii) by conditionally deleting *Musk* in muscle fibers by muscle creatine kinase-driven Cre, which

352 caused death of the mice at approximately one month of age (*23*).

353 AAVMYO-CRISPR/Cas9 knockdown of *Musk*, *Acvr2a* and *Acvr2b* when injected systemically or at

354 the highest dose into TA muscle resulted in a systemic loss of the targeted proteins. The systemic effect

355 of the high intramuscular doses is likely based on the body-wide spreading of the sgRNA-expressing

356 recombinant viruses *via* the blood stream and the subsequent transduction of skeletal muscles.

357 Systemically administered AAVMYO targets all muscles but has the highest transduction rate in the

358 diaphragm (Fig. 4C,(*7, 8*)). While such body-wide spreading may not be a problem for most

359 experiments, in case of *Musk* deletion, NMJs deteriorate and muscles become denervated (*23*). At the

360 highest dose of 3 x 10^{11} vg/mouse (corresponding to approx. 1.3 x 10^{13} vg/kg), mice started to lose

361 weight 14 days post-injection and reached euthanization criteria (20% weight loss) at 3 weeks (Fig. 6B).

362 Examination of the diaphragm muscle indicated NMJ deterioration. Based on this, mice injected with

363 the highest dose needed to be analyzed already at 3 weeks post-injection, which explains the less

364 severe phenotype in the hindlimbs. Lowering the dose of the injected virus to 3 or 1 x 10^{10} vg/mouse

365 largely prevented weight and muscle mass loss in the contralateral leg while the injected muscle still

366 showed all signs of NMJ deterioration and denervation. Thus, with the proper administration and viral

367 titer, the AAVMYO-CRISPR/Cas9 method also allows for locally restricted perturbation of muscle

368 function.

369 We also demonstrate efficacious, simultaneous inactivation of multiple genes (*Acvr2a* and *Acvr2b*)

370 with this system, opening the possibility of studying several genes or signaling pathways concurrently.

371 Although our experiments targeting *Prkca* indicate that one sgRNA can be sufficient to eliminate a

372 gene, testing each sgRNA *in vitro* prior to *in vivo* application is laborious. Hence, we suggest targeting

373 each gene with two to three different sgRNAs, minimizing the risk of insufficient protein loss. Since one

374 AAV has sufficient packaging capacity for at least 7 sgRNAs, three genes can be silenced with one AAV.

375 By delivering two AAVs (as done here for *Acvr2a* and *Acvr2b*), up to six independent genes could be

376 silenced simultaneously, allowing interrogation of entire signaling pathways, specifically in skeletal

377 muscle fibers.

378 In summary, we conclusively demonstrate that AAVMYO-mediated delivery of sgRNA to Cas9-

379 expressing skeletal muscle fibers allows fast, efficient and specific gene knockouts. The multiplexable

380 nature and capacity to induce systemic or local gene editing further strengthens the universality of the

381 system. Therefore, this system provides an invaluable resource to perform loss-of-function studies in

382 skeletal muscle fibers compared to traditional knockout mouse models and promises to greatly

383   accelerate the interrogation of novel gene targets with a much reduced number of animals needed

384   and thus will strongly contribute to our understanding of skeletal muscle biology.

385   Material and Methods:

386   **Mice**

387   All procedures involving animals were performed in accordance with Swiss regulations and approved

388   by the veterinary commission of the canton Basel Stadt. CRISPR/Cas9 knockin mice (*11*) were crossed

389   with HSA-Cre (*13*) or HSA-Mer-Cre-Mer mice (*12*) to generate Cas9mKI or iCas9mKI, respectively.

390   Littermates, knockin for Cas9 but not expressing Cre recombinase, were used as controls.

391   **Cell culture C2C12**

392   Murine C2C12 myoblasts were cultured in growth medium (DMEM (Gibco) supplemented with 10%

393   fetal bovine serum (Biological Industries) and 1% penicillin/streptomycin (Sigma)) at 37°C in an

394   atmosphere of 5% CO_2. After reaching 70% confluence, cells were transiently transfected using

395   Lipofectamine 2000 (Invitrogen), according to the manufacturer's protocol. At 48 h post-transfection,

396   cells were incubated in growth medium, supplemented with 3 µg/ml puromycin (Sigma), for another

397   48 h to select for transfected cells. After selected cells reached confluence, cells were incubated in

398   differentiation medium (DMEM (Gibco) supplemented with 2% horse serum (Biological Industries) and

399   1% penicillin/streptomycin for 5 days to induce formation of multinucleated myotubes.

400   **AAV administration**

401   Prior to AAV administration, mice were anaesthetized by isoflurane inhalation. For intramuscular

402   injection, the TA or TA and GAS muscle of adult mice (older than 6 weeks) was injected with 50 µL of

403   AAV (3 x 10^{11} vg, if not stated differently) in PBS. For intravenous injection, 100 µL of AAV (1 x 10^{14}

404   vg/kg) in PBS were injected into the lateral tail vein of 6-week-old mice. For targeting of PKCα or

405   Acvr2a/Acvr2b, PBS or non-targeting AAV-injected control or Cas9mKI mice were used as control. For

406   targeting of Musk, PBS-injected Cas9mKI mice or AAVMYO-7sgMusk-injected control mice were used

407   as control.

408   **Denervation**

409   Mice were anaesthetized by isoflurane inhalation 6 weeks post-AAV administration. After making a

410   small incision on the skin between sciatic notch and knee, the sciatic nerve was exposed by gentle

411   separation of muscles under the skin. The nerve was then lifted using a glass hook and disrupted by

412   removing a 5 mm piece. The wound was closed by surgical clips and mice were returned to their cage.

413   Mice were treated with Buprenorphine (0.1 mg/kg of body weight) one hour before and for two days

414   after operation.

415   **sgRNA design and AAV vectors**

416   The sgRNAs, listed in Table 1 were selected using CRISPOR (*19*) to minimize off-target effects and

417   assembled as previously described using the multiplex CRISPR/Cas9 assembly kit (*49*). An array of three

418   or seven human U6/sgRNA cassettes were cloned into an AAV transfer vectors. The AAV transfer

419   vectors used for 3-plex sgRNA delivery into skeletal muscle were cloned between AAV serotype 2 ITR's

420   including a cloning site for multiplexed hU6-sgRNA insertions (MluI and KpnI (NEB)), the ubiquitous

421   CMV promoter, tdTomato, WPRE and bovine growth hormone polyA signal. For 7-plex sgRNA delivery

422   by AAV, the CMV-tdTomato-WPRE sequence was removed from the AAV transfer vector.

423   For in vitro CRISPR applications, sgRNAs were cloned into an all-in-one CRISPR/Cas9 vector using BbsI

424   (NEB). The all-in-one CRISPR/Cas9 vector was cloned between AAV serotype 2 ITRs including a human

425   U6 promoter, sgRNA scaffold, an EFS promoter, SpCas9 linked to puromycin N-acetyltransferase via a

426   GSG-P2A linker and bovine growth hormone polyA signal. Complete vector maps and sequences are

427   available upon request.

AAV production, purification and titration

The AAV-sgRNA plasmid vectors were used for AAV production and purification. Briefly, adherent HEK293T cells were transiently transfected with transfer (AAV-sgRNA construct), AAV helper (AAV9 (a gift of J. M. Wilson Addgene, plasmid # 112867), AAVMYO (*7*), AAVMYO2 (*8*) or AAVMYO3 (*8*)) and pAdDeltaF6 helper (a gift from J. M. Wilson Addgene, plasmid # 112867) plasmid using PEI MAX (Polyscience). For small or large AAV preparations, ten or twenty HEK293T confluent 15 cm tissue culture plates were processed, respectively. The supernatant was collected 48 and 72 h post-transfection and cells were dislodged 72 hours post-transfection in PBS. Cells were centrifuged at 500g at 4°C for 10 min and resuspended in AAV lysis solution (50 mM Tris-HCl, 1 M NaCl, 10 mM NgCl$_2$, pH 8.5). 50 U of salt active nuclease (Sigma) was added per harvested 15 cm dish and incubated at 37°C for 1 h with continuous shaking. The lysate was spun at 4000g at 4°C for 15 min and supernatant was collected. AAV particles from the supernatant were precipitated by adding polyethylene glycol 8000 (Sigma) to a final concentration of 8% (w/v), incubated for 2h at 4°C and then spun at 4000g at 4°C for 30 min. The supernatant was discarded, while the pellet was resuspended in AAV lysis buffer and pooled with the cell lysate. AAV particles were purified by using a 15-25-40-60% iodixanol (Serumwerk) gradient. The gradient was centrifuged at 63000 rpm (Beckman type 70 Ti rotor) for 2 h at 4°C and the AAV particles were collected from the 40-60% phase interface. The extract was passed through a 100 kDa MWCO filter (Millipore) and washed with PBS supplemented with 0.01% Pluronic F-68 surfactant (Gibco) until buffer was exchanged completely. The final volume was decreased to reach a final AAV concentration of > 1 x 10^{13} vg/ml. Virus was tittered using RT-qPCR targeted to the ITRs, as previously described (*50*), using a PvuII (NEB) -linearized plasmid standard. Primers used for titration are listed in Table 1.

Protein isolation and Western blot analysis

Dissected muscles were snap-frozen in liquid nitrogen and pulverized. Proteins were extracted using RIPA lysis buffer (50 mM Tris-HCl pH 8.0, 150 mM NaCl, 1% NP-40, 0.5% sodium deoxycholate, 0.1% SDS) supplemented with protease and phosphatase inhibitors (both Roche) for 2 h at 4°C, followed by sonication. Lysates were centrifuged at 16000g for 20 min at 4°C and Pierce BCA Protein Assay Kit (Thermo Fisher Scientific) was used to determine cleared lysate concentration. Equalized protein samples were separated on 4-12% Bis-Tris Protein Gels (NuPage Novex), followed by transfer to nitrocellulose membranes (GE Healthcare Life Science). Membranes were blocked for 1 h by 5% BSA in PBS-T (1% Tween-20) and incubated with primary antibody in blocking solution overnight at 4°C. After 3 washes with PBS-T, membranes were incubated with secondary horseradish peroxidase-conjugated antibody for 1 h at RT. After washing 3 times with PBS-T, proteins were visualized using KPL LumiGLO (Seracare) and cheminumilescence was captured by a Fusion Fx machine (ViberLourmat).

462 Protein abundance was quantified using the FusionCapt Advance software with linear background

463 subtraction. Used antibodies are listed in Table 2.

Immunostaining of muscle cross sections and muscle histology analysis

465 Animal tissue was dissected, prepared and sectioned for immunohistochemistry as previously

466 described (*51*). Tissue for analysis of cytosolic expression of GFP or tdTomato was directly fixed in ice-

467 cold 4% PFA (Electron Microscopy Science) for 2 h at 4°, followed by dehydration with 20% sucrose

468 (Sigma) in PBS at 4°C overnight. The next day, tissue was processed like non-fixed tissue as previously

469 described (*51*). TA muscle cross sections were blocked and permeabilized for 30 min at RT with 3%

470 BSA, 0.5% Triton X-100 in PBS. Primary antibodies were diluted in blocking solution for 2 h at RT.

471 Sections were washed with PBS three times before being incubated in secondary antibody solution for

472 1 h at RT. All antibodies are listed in Table 2. Sections were washed with PBS four times and mounted

473 with ProLong Gold Antifade Mountant (Invitrogen). Muscle sections were imaged at the Biozentrum

474 Imaging Core Facility with a SpinD confocal microscope (Olympus). The previously described script for

475 automated muscle cross section analysis (*52*) was further developed in-house and is available upon

476 request.

Whole-mount NMJ staining

478 EDL muscles were fixed, cut into bundles and prepared for NMJ staining as previously described (*51*).

479 The presynapse was visualized using a primary antibody mix against neurofilament and synaptic vesical

480 protein, while the postysnapse was stained using A647-conjugated α-bungarotoxin. NMJs were imaged

481 at the Biozentrum Imaging Core Facility with a SpinD confocal microscope (Olympus).

In vitro muscle force

483 Fast-twitch EDL and slow-twitch SOL muscles were carefully isolated for in vitro force and fatigue test

484 as previously described (*51*). The measurement was carried out on the 1200 A Isolated Muscle System

485 (Aurora Scientific) in Ringer solution (137 mM NaCl, 24 mM NaHCO$_3$, 11 mM glucose, 5 mM KCl, 2 mM

486 CaCl$_2$, 1 mM MgSO$_4$, 1 mM NaH$_2$PO$_4$) which was gassed with 95% O$_2$, 5% CO$_2$ and kept at 30 °C.

Genomic DNA isolation, PCR amplification and TIDE

488 Cells were washed in PBS, while dissected tissue was snap-frozen in liquid nitrogen and pulverized in

489 liquid nitrogen. Genomic DNA from cells or tissue was isolated using the DNeasy blood and Tissue kit

490 (Qiagen) according to the manufacturer's protocol. DNA was amplified using standard PCR using

491 LongAmp Taq DNA polymerase (NEB) targeting the CRISPR locus with a 200-500 bp long amplicon.

492 Used primers are listed in Table 1. PCR amplicons were purified using AMPure XP beads (Beckman) and

493 Sanger-sequenced using one of the two PCR primers (Microsynth). TIDE was applied to sequencing

494 chromatograms to assess CRISPR editing efficiency of the target locus (*53*).

Amplicon deep sequencing analysis

496 PCR of genomic DNA was performed using LongAmp Taq DNA polymerase (NEB) and primers designed

497 against an amplicon of 200-500 bp targeting the CRISPR-locus and the top four CRISPOR-predicted off-

498 targets. First-round PCR primers contained adapter sequence for DNA/RNA UD Indexes (Illumina). The

499 second round of PCR and pooling of samples was performed according to the Illumina Nextera DNA

500 library prep guide. Pooled amplicons were sequenced with standard 500 cycles kit PE 2x251 on an

501 Illumina MiSeq instrument. Samples were demultiplexed according to assigned barcodes and FASTQ

502 files were analyzed using the CRISPResso2 software package (*54*).

AAV genome copy number quantification

504 The AAV viral genome copy number per nuclei was determined by RT-qPCR using PowerUp SYBR Green

505 Master Mix (Applied Biosystems) and primers (Table 1) targeting the tdTomato-WPRE sequence (AAV)

506 or the R26 locus (nuclei) on a QuantStudio5 (Applied Biosystems) instrument. The cycle threshold (CT)

507 values were converted into copy numbers by measuring against a standard curve of the AAV transfer

508 plasmid or the Ai9 plasmid (a gift from H. Zeng Addgene plasmid # 22799). The AAV genome copy

509 number was divided by the number of nuclei to normalize for tissue input.

RT-qPCR

511 Pulverized muscle tissue was lysed in RLT buffer (Qiagen) and RNA was extracted using the RNeasy®

512 Mini Kit for fibrous tissue (Qiagen). cDNA was reverse transcribed using the iScript™ cDNA synthesis

513 kit (Bio-Rad) and 500 ng of RNA according to the manual. RT-qPCR was performed using PowerUp SYBR

514 Green Master Mix (Applied Biosystems) and target specific primers (table 1) on a QuantStudio5

515 (Applied Biosystems) instrument. Data were analyzed using the comparative CT method ($2^{-\Delta\Delta Cq}$). Raw

516 CT values of targets were normalized to CT values of a housekeeper (Tata-box-binding protein), which

517 was stable between conditions, and then further normalized to the control group for visualization.

Statistical analysis:

519 All values are expressed as mean +/- SEM, unless stated otherwise. Data were analyzed in GraphPad

520 Prism 8. Unpaired Student t tests were used for pairwise comparison. One-way ANOVAs with Fisher's

521 LSD post-hoc tests were used to compare between three groups, while Tukey post-hoc tests were used

522 for comparison between more than three groups, so long as the ANOVA reached statistical

523 significance. Significant differences (*$P < 0.05$, **$P < 0.01$, *** $P < 0.001$) are reported on figures, where

524 appropriate.

Titration	
ITR_F	GGAACCCCTAGTGATGGAGTT
ITR_R	CGGCCTCAGTGAGCGA
sgRNA	
sgRNA_NT_1	CGGAAGAGCGAGCTCTTCT
sgRNA_Prkca_1	ACGCCGTGGAGTCGTTGGCC
sgRNA_Prkca_2	TGATGAAAAGCTCCACGTCA
sgRNA_Acvr2a_1	AGAGCAAGAGATAAGAAAGA
sgRNA_Acvr2a_2	AGAGACAGAACCAACCAGAC
sgRNA_Acvr2a_3	AGCAACAAAAGTACACTTCA
sgRNA_Acvr2a_4	AGCAGAATGTTGTAATAGGG
sgRNA_Acvr2a_5	GAGTAGGAACAAGTACAGGA
sgRNA_Acvr2a_6	GCTGTTAGAAGTGAAAGCAA
sgRNA_Acvr2a_7	AGAGAAAAGAGGCACCAGTG
sgRNA_Acvr2b_1	GCAGCAGCAGAAGTACACCT
sgRNA_Acvr2b_2	CGTCATCGGAAGCCTCCCTA
sgRNA_Acvr2b_3	CTGGAGCGCACCAACCAGAG
sgRNA_Acvr2b_4	AGTGGCTTCAGGCCCACCAG
sgRNA_Acvr2b_5	TTCATTGCTGCCGAGAAACG
sgRNA_Acvr2b_6	GTGGAACGAACTGTGCCACG
sgRNA_Acvr2b_7	ACCATCGAGCTGGTGAAGAA
sgRNA_Musk_1	AAGAGGCGTGGTGATGACAG
sgRNA_Musk_2	CTTCCACGCTCAGAATGGTG
sgRNA_Musk_3	ATCTGTGTCCTGGATCAAGG

sgRNA_Musk_4	TGCAGGACAGTACCGCTGTG
sgRNA_Musk_5	AGTCCCGCTGAAGGCAACCA
sgRNA_Musk_6	CAGGGCACCACAACTCTCCA
sgRNA_Musk_7	TAGGGTTACAAAGGAACCAA
TIDE	
Prkca_TIDE_F	GAGAGAGCCAGAGAGAGCG
Prkca_TIDE_R	CAGATGAAGTCGGTGCAGTG
AAV genome copy number	
tdT_WPRE_F	CTGTTCCTGTACGGCATGG
tdT_WPRE_R	GGCATTAAAGCAGCGTATCC
R26_F	GTGGAGCCGTTCTGTGAGAC
R26_R	CTTTTCCGCTCCCTTCTCCC
Amplicon NGS	
Prkca_Ontarget_F	TCGTCGGCAGCGTCAGATGTGTATAAGAGACAGGAGAGAGCCAGAGAGAGCG
Prkca_Ontarget_R	GTCTCGTGGGCTCGGAGATGTGTATAAGAGACAGCAGATGAAGTCGGTGCAGTG
Prkca_Offtarget1_F	TCGTCGGCAGCGTCAGATGTGTATAAGAGACAGACCATCCCCTCAGAAGAGAC
Prkca_Offtarget1_R	GTCTCGTGGGCTCGGAGATGTGTATAAGAGACAGTCCTGTAGCTCCTAGGATGC
Prkca_Offtarget2_F	TCGTCGGCAGCGTCAGATGTGTATAAGAGACAGGGGGGCAATTGGGCATTTAAT
Prkca_Offtarget2_R	GTCTCGTGGGCTCGGAGATGTGTATAAGAGACAGGTACAACAGGGAGCCTTTCC
Prkca_Offtarget3_F	TCGTCGGCAGCGTCAGATGTGTATAAGAGACAGGTGGTCACTCGATTCCACTC
Prkca_Offtarget3_R	GTCTCGTGGGCTCGGAGATGTGTATAAGAGACAGGCACTCTGGACCTAGGAGAT
Prkca_Offtarget4_F	TCGTCGGCAGCGTCAGATGTGTATAAGAGACAGATGCAATACAGCTTCCCTGG
Prkca_Offtarget4_R	GTCTCGTGGGCTCGGAGATGTGTATAAGAGACAGACACGGGGAGGAGATAAACA
RT-qPCR	

Musk_F	GCTCCTGAATCCCACAATGTC
Musk_R	AGAGTCCTGGCTTTGTGATGA
Acvr2a_F	CAATACAGGACAAACAGTCCT
Acvr2a_R	GAACTGTAGTATGTTCTCATG C
Acvr2b_F	ATACCCATGGACAGGTTGG
Acvr2b_R	ATGTCGATACGCAGGAAGG
Chrng_F	GCCCTGGAGTCAGCTATGAG
Chrng_R	GGTAAAACCTTGCCCAGTCA
Chrna1_F	GCCATTAACCCGGAAAGTGAC
Chrna1_R	CCCCGCTCTCCATGAAGTT
Gadd45a_F	CCGAAAGGATGGACACGGTG
Gadd45a_R	TTATCGGGGTCTACGTTGAGC

Table 1: List of used primers and sgRNAs

Western Blot			
PKCa	1:1000	2056S	Cell Signaling
FLAG	1:1000	F3165	Sigma
tdTomato	1:5000	orb182397	Biorbyt
GFP	1:1000	11814460001	Roche
GAPDH	1:5000	2118	Cell Signaling
HDAC4	1:1000	7628S	Cell Signaling
Goat anti-rabbit HRP	1:10000	111-035-003	Jackson Immuno
Goat anti-mouse HRP	1:10000	115-035-003	Jackson Immuno
Donkey anti-goat HRP	1:10000	705-035-003	Jackson Immuno
Immunostaining			
GFP	1:400	A10262	Molecular Probes
MHC1	1:50	BA-D5	DSHB
MHC2a	1:200	SC-71	DSHB
MHC2b	1:100	BF-F3	DSHB
Laminin	1:200	L9393	DSHB
Goat anti-mouse 405	1:50	115-475-207	Jackson Immuno
Goat anti-mouse 568	1:200	A-21124	Invitrogen
Goat anti-mouse 488	1:200	A-21042	Invitrogen
Donkey anti-rabbit 647	1:300	711-605-152	Jackson Immuno
Donkey anti-chicken 488	1:500	703-545-155	Jackson Immuno
DAPI	1:2000	D9542	Sigma
Whole mount immunostaining			
Neurofilament	1:2000	2H3	DSHB

Synaptic vesicle protein	1:400	SV2	DSHB
αBTX 647	1:500	B-35450	Invitrogen
Goat anti-mouse 555	1:500	A-21127	Invitrogen

526 **Table 2: List of used antibodies**

527 <u>Acknowledgments:</u>

535 **Author contributions**

536 Conceptualization: MT, MAR; methodology: MT; investigations: MT, SL, FO; statistical analysis: MT;

537 visualization: MT; supervision: MAR, RJP, DG; writing original draft: MT, MAR; writing review and

538 editing: MT, DG, MAR; funding acquisition: MAR

539 Corresponding author: MAR

540 **Competing interests**

541 Authors declare that they have no competing interests.

542 **Data and materials availability**

543 All data are available in the main text or the supplementary materials.

544 References:

545 1. M. Adli, The CRISPR tool kit for genome editing and beyond. *Nature communications* **9**, 1911
546 (2018).

547 2. J. C. Bruusgaard, K. Liestol, M. Ekmark, K. Kollstad, K. Gundersen, Number and spatial
548 distribution of nuclei in the muscle fibres of normal mice studied in vivo. *J Physiol* **551**, 467-
549 478 (2003).

550 3. B. Hu *et al.*, Therapeutic siRNA: state of the art. *Signal Transduct Target Ther* **5**, 101 (2020).

551 4. X. C. Kong, P. Barzaghi, M. A. Ruegg, Inhibition of synapse assembly in mammalian muscle in
552 vivo by RNA interference. *EMBO Rep* **5**, 183-188 (2004).

553 5. M. Sandri *et al.*, Foxo transcription factors induce the atrophy-related ubiquitin ligase
554 atrogin-1 and cause skeletal muscle atrophy. *Cell* **117**, 399-412 (2004).

555 6. D. R. Bisset *et al.*, Therapeutic impact of systemic AAV-mediated RNA interference in a
556 mouse model of myotonic dystrophy. *Hum Mol Genet* **24**, 4971-4983 (2015).

557 7. J. Weinmann *et al.*, Identification of a myotropic AAV by massively parallel in vivo evaluation
558 of barcoded capsid variants. *Nature communications* **11**, 5432 (2020).

559 8. J. El Andari *et al.*, Semirational bioengineering of AAV vectors with increased potency and
560 specificity for systemic gene therapy of muscle disorders. *Sci Adv* **8**, eabn4704 (2022).

561 9. M. Tabebordbar *et al.*, Directed evolution of a family of AAV capsid variants enabling potent
562 muscle-directed gene delivery across species. *Cell* **184**, 4919-4938 e4922 (2021).

563 10. M. J. Petrany *et al.*, Single-nucleus RNA-seq identifies transcriptional heterogeneity in
564 multinucleated skeletal myofibers. *Nature communications* **11**, 6374 (2020).

565 11. R. J. Platt *et al.*, CRISPR-Cas9 knockin mice for genome editing and cancer modeling. *Cell* **159**,
566 440-455 (2014).

567 12. J. J. McCarthy, R. Srikuea, T. J. Kirby, C. A. Peterson, K. A. Esser, Inducible Cre transgenic
568 mouse strain for skeletal muscle-specific gene targeting. *Skelet Muscle* **2**, 8 (2012).

569 13. M. Leu *et al.*, Erbb2 regulates neuromuscular synapse formation and is essential for muscle
570 spindle development. *Development (Cambridge, England)* **130**, 2291-2301 (2003).

571 14. V. Thomanetz *et al.*, Ablation of the mTORC2 component rictor in brain or Purkinje cells
572 affects size and neuron morphology. *J Cell Biol* **201**, 293-308 (2013).

573 15. S. Sarin *et al.*, Role for Wnt Signaling in Retinal Neuropil Development: Analysis via RNA-Seq
574 and In Vivo Somatic CRISPR Mutagenesis. *Neuron* **98**, 109-126 e108 (2018).

575 16. C. F. Bentzinger *et al.*, Skeletal muscle-specific ablation of raptor, but not of rictor, causes
576 metabolic changes and results in muscle dystrophy. *Cell Metab* **8**, 411-424 (2008).

577 17. C. L. Bell *et al.*, The AAV9 receptor and its modification to improve in vivo lung gene transfer
578 in mice. *J Clin Invest* **121**, 2427-2435 (2011).

579   18.   H. Zhu, T. Wang, R. John Lye, B. A. French, B. H. Annex, Neuraminidase-mediated
580   desialylation augments AAV9-mediated gene expression in skeletal muscle. *J Gene Med* **20**,
581   e3049 (2018).

582   19.   J. P. Concordet, M. Haeussler, CRISPOR: intuitive guide selection for CRISPR/Cas9 genome
583   editing experiments and screens. *Nucleic Acids Res* **46**, W242-W245 (2018).

584   20.   H. Lin *et al.*, Decoding the transcriptome of denervated muscle at single-nucleus resolution. *J
585   Cachexia Sarcopenia Muscle* **13**, 2102-2117 (2022).

586   21.   L. A. Tintignac, H. R. Brenner, M. A. Ruegg, Mechanisms Regulating Neuromuscular Junction
587   Development and Function and Causes of Muscle Wasting. *Physiol Rev* **95**, 809-852 (2015).

588   22.   T. M. DeChiara *et al.*, The receptor tyrosine kinase MuSK is required for neuromuscular
589   junction formation in vivo. *Cell* **85**, 501-512 (1996).

590   23.   B. A. Hesser, O. Henschel, V. Witzemann, Synapse disassembly and formation of new
591   synapses in postnatal muscle upon conditional inactivation of MuSK. *Mol Cell Neurosci* **31**,
592   470-480 (2006).

593   24.   W. Hoch *et al.*, Auto-antibodies to the receptor tyrosine kinase MuSK in patients with
594   myasthenia gravis without acetylcholine receptor antibodies. *Nature medicine* **7**, 365-368
595   (2001).

596   25.   V. Witzemann, H. R. Brenner, B. Sakmann, Neural factors regulate AChR subunit mRNAs at
597   rat neuromuscular synapses. *J Cell Biol* **114**, 125-141 (1991).

598   26.   S. J. Lee, Myostatin: A Skeletal Muscle Chalone. *Annu Rev Physiol*, (2022).

599   27.   A. C. McPherron, A. M. Lawler, S. J. Lee, Regulation of skeletal muscle mass in mice by a new
600   TGF-beta superfamily member. *Nature* **387**, 83-90 (1997).

601   28.   L. Grobet *et al.*, A deletion in the bovine myostatin gene causes the double-muscled
602   phenotype in cattle. *Nat Genet* **17**, 71-74 (1997).

603   29.   M. Schuelke *et al.*, Myostatin mutation associated with gross muscle hypertrophy in a child.
604   *N Engl J Med* **350**, 2682-2688 (2004).

605   30.   S. J. Lee *et al.*, Functional redundancy of type I and type II receptors in the regulation of
606   skeletal muscle growth by myostatin and activin A. *Proc Natl Acad Sci U S A* **117**, 30907-
607   30917 (2020).

608   31.   S. Welle, K. Bhatt, C. A. Pinkert, R. Tawil, C. A. Thornton, Muscle growth after
609   postdevelopmental myostatin gene knockout. *Am J Physiol Endocrinol Metab* **292**, E985-991
610   (2007).

611   32.   H. Amthor *et al.*, Muscle hypertrophy driven by myostatin blockade does not require
612   stem/precursor-cell activity. *Proc Natl Acad Sci U S A* **106**, 7479-7484 (2009).

613   33.   A. Briguet, I. Courdier-Fruh, M. Foster, T. Meier, J. P. Magyar, Histological parameters for the
614   quantitative assessment of muscular dystrophy in the mdx-mouse. *Neuromuscul Disord* **14**,
615   675-682 (2004).

616   34.   R. D. Chow *et al.*, AAV-mediated direct in vivo CRISPR screen identifies functional suppressors
617   in glioblastoma. *Nature neuroscience* **20**, 1329-1341 (2017).

618   35.   T. Katsuda *et al.*, Rapid in vivo multiplexed editing (RIME) of the adult mouse liver.
619   *Hepatology*, (2022).

620   36.   M. Tabebordbar *et al.*, In vivo gene editing in dystrophic mouse muscle and muscle stem
621   cells. *Science* **351**, 407-411 (2016).

622   37.   L. He *et al.*, CRISPR/Cas9/AAV9-mediated in vivo editing identifies MYC regulation of 3D
623   genome in skeletal muscle stem cell. *Stem Cell Reports* **16**, 2442-2458 (2021).

624   38.   L. Amoasii *et al.*, Single-cut genome editing restores dystrophin expression in a new mouse
625   model of muscular dystrophy. *Sci Transl Med* **9**, (2017).

626   39.   D. U. Kemaladewi *et al.*, Correction of a splicing defect in a mouse model of congenital
627   muscular dystrophy type 1A using a homology-directed-repair-independent mechanism.
628   *Nature medicine* **23**, 984-989 (2017).

629   40.   Y. Zhang *et al.*, Enhanced CRISPR-Cas9 correction of Duchenne muscular dystrophy in mice by
630   a self-complementary AAV delivery system. *Sci Adv* **6**, eaay6812 (2020).

631   41.   C. E. Nelson *et al.*, In vivo genome editing improves muscle function in a mouse model of
632   Duchenne muscular dystrophy. *Science* **351**, 403-407 (2016).

633   42.   L. Amoasii *et al.*, Gene editing restores dystrophin expression in a canine model of Duchenne
634   muscular dystrophy. *Science* **362**, 86-91 (2018).

635   43.   N. S. McCarty, A. E. Graham, L. Studena, R. Ledesma-Amaro, Multiplexed CRISPR technologies
636   for gene editing and transcriptional regulation. *Nature communications* **11**, 1281 (2020).

637   44.   H. Schmalbruch, U. Hellhammer, The number of nuclei in adult rat muscles with special
638   reference to satellite cells. *Anat Rec* **189**, 169-175 (1977).

639   45.   M. Bengtsen *et al.*, Comparing the epigenetic landscape in myonuclei purified with a PCM1
640   antibody from a fast/glycolytic and a slow/oxidative muscle. *PLoS Genet* **17**, e1009907
641   (2021).

642   46.   A. M. Chakrabarti *et al.*, Target-Specific Precision of CRISPR-Mediated Genome Editing. *Mol
643   Cell* **73**, 699-713 e696 (2019).

644   47.   M. Dos Santos *et al.*, Single-nucleus RNA-seq and FISH identify coordinated transcriptional
645   activity in mammalian myofibers. *Nature communications* **11**, 5102 (2020).

646   48.   A. R. Punga, M. Maj, S. Lin, S. Meinen, M. A. Ruegg, MuSK levels differ between adult skeletal
647   muscles and influence postsynaptic plasticity. *Eur J Neurosci* **33**, 890-898 (2011).

648   49.   T. Sakuma, A. Nishikawa, S. Kume, K. Chayama, T. Yamamoto, Multiplex genome engineering
649   in human cells using all-in-one CRISPR/Cas9 vector system. *Sci Rep* **4**, 5400 (2014).

650   50.   F. Wang, X. Cui, M. Wang, W. Xiao, R. Xu, A reliable and feasible qPCR strategy for titrating
651   AAV vectors. *Medical science monitor basic research* **19**, 187-193 (2013).

652   51.   D. J. Ham *et al.*, The neuromuscular junction is a focal point of mTORC1 signaling in
653   sarcopenia. *Nature communications* **11**, 4510 (2020).

654   52.   L. Encarnacion-Rivera, S. Foltz, H. C. Hartzell, H. Choo, Myosoft: An automated muscle
655   histology analysis tool using machine learning algorithm utilizing FIJI/ImageJ software. *PLoS*
656   *One* **15**, e0229041 (2020).

657   53.   E. K. Brinkman, T. Chen, M. Amendola, B. van Steensel, Easy quantitative assessment of
658   genome editing by sequence trace decomposition. *Nucleic Acids Res* **42**, e168 (2014).

659   54.   K. Clement *et al.*, CRISPResso2 provides accurate and rapid genome editing sequence
660   analysis. *Nat Biotechnol* **37**, 224-226 (2019).
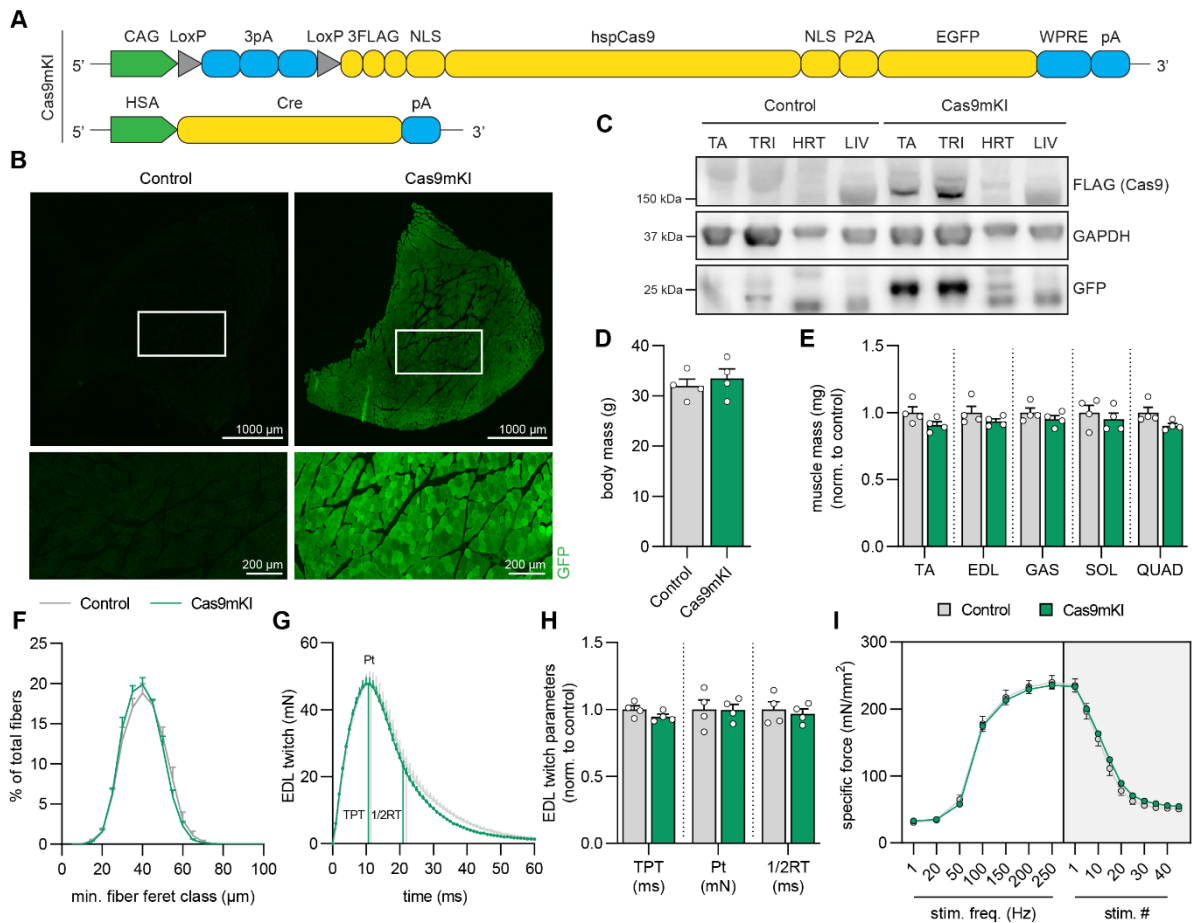
Figure 1: Validation of Cas9mKI mice. (A) Schematic of the Cas9mKI mouse model. Abbreviations are: CAG: cytomegalovirus (CMV) enhancer fused to the chicken beta-actin promoter; LoxP: locus of X-over P1; pA: polyadenylation signal; FLAG: FLAG-tag; NLS: nuclear localization signal; hspCas9: humanized *Streptococcus pyogenes* Cas9; P2A: 2A self-cleaving peptide; EGFP: enhanced green fluorescent protein; WPRE: woodchuck hepatitis virus post-transcriptional regulatory element; HSA: human α-skeletal actin; Cre: Cre recombinase. (B) Cross-sections of *tibialis anterior* (TA) muscle stained for EGFP (green) in control and Cas9mKI mice. (C) Western blot analysis of lysates from TA, *triceps brachii* (TRI), heart (HRT) and liver (LIV) of control and Cas9mKI mice using antibodies against the FLAG-tag, GFP or glyceraldehyde-3-phosphate dehydrogenase (GAPDH). Only TA and TRI muscles of Cas9mKI mice are positive for the FLAG-tag and GFP; no expression was detected in HRT or LIV. (D) Body mass of 19-week-old control and Cas9mKI mice. (E) Relative mass of *soleus* (SOL), *extensor digitorum longus* (EDL), TA, *gastrocnemius* (GAS) and *quadriceps* (QUAD) muscles from control and Cas9mKI mice. (F) Minimal fiber feret distribution of muscle fibers from TA of control and Cas9mKI mice. (G) Ex-vivo twitch response of isolated EDL muscle from Cas9mKI and control mice. Peak twitch (Pt), time-to-peak twitch (TPT) and half-relaxation time (1/2RT) are indicated. (H) Quantification of ex-vivo twitch response parameters (TPT, Pt, 1/2RT) of isolated EDL muscle from Cas9mKI and control mice. (I) Force-frequency

679   curve (left) and fatigue response to multiple stimulations (right) of EDL muscle from control and

680   Cas9mKI mice. Data are means ± SEM. N = 4 (mice). None of the data are significantly different between

681   control and Cas9mKI mice (P > 0.05) using unpaired t-test.
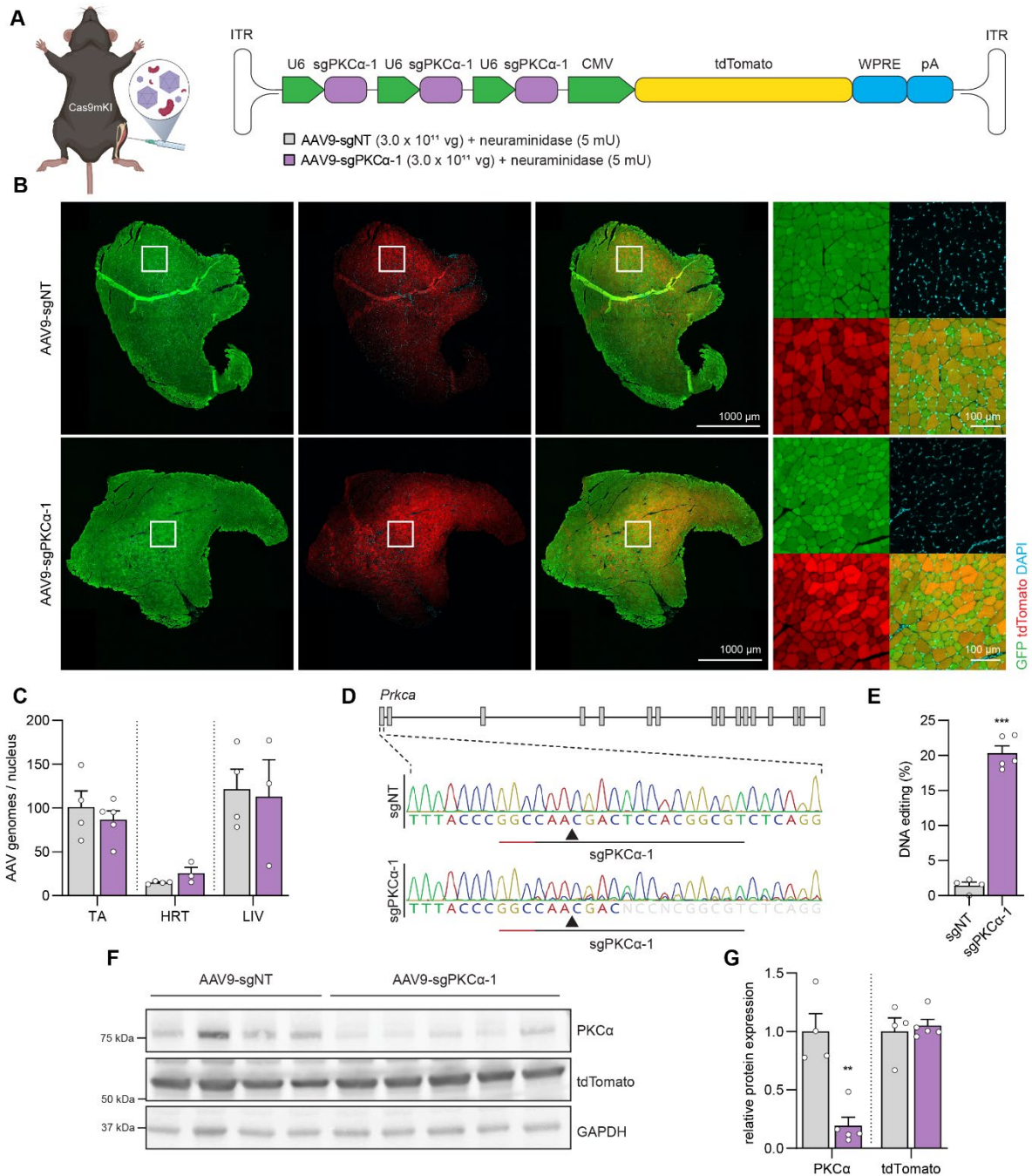
Figure 2: Knock out of *Prkca* in TA muscle upon AAV9/neuraminidase-mediated delivery of sgRNA to Cas9mKI mice. (A) Schematic illustration of experimental procedure and targeting construct. For abbreviations, see legend to Figure 1. (B) Cross-section of *tibialis anterior* (TA) muscle stained for Cas9/GFP (green), tdTomato (red) and DAPI (blue) 6 weeks after injection of neuraminidase plus AAV9-sgNT or AAV9-sgPKCα-1. (C) Quantification of AAV genomes per nucleus in TA muscle, heart (HRT) and liver (LIV) in AAV9-sgNT (grey) and AAV9-sgPKCα-1-injected (purple) mice. (D) Illustration of the *Prkca* gene and representative Sanger sequencing chromatograms at the sgPKCα-1 target site (underlined) of AAV9-sgNT and AAV9-sgPKCα-1-injected TA muscle. Note that sequencing becomes ambiguous in sgPKCα-1-expressing mice, indicative of genome editing. (E) Total INDEL formation analysis by TIDE of

692   TA muscle injected with AAV9-sgNT and AAV9-sgPKCα-1. (F) Western blot analysis and (G)

693   quantification of PKCα and tdTomato expression in TA muscle 6 weeks post-injection with AAV9-sgNT

694   (grey) or AAV9-sgPKCα-1 (purple). Data are means ± SEM. N = 4 (sgNT) and 5 (sgPKCα-1) mice.

695   Statistical analysis used unpaired t-test. *P < 0.05, **P< 0.01, ***P < 0.001 .
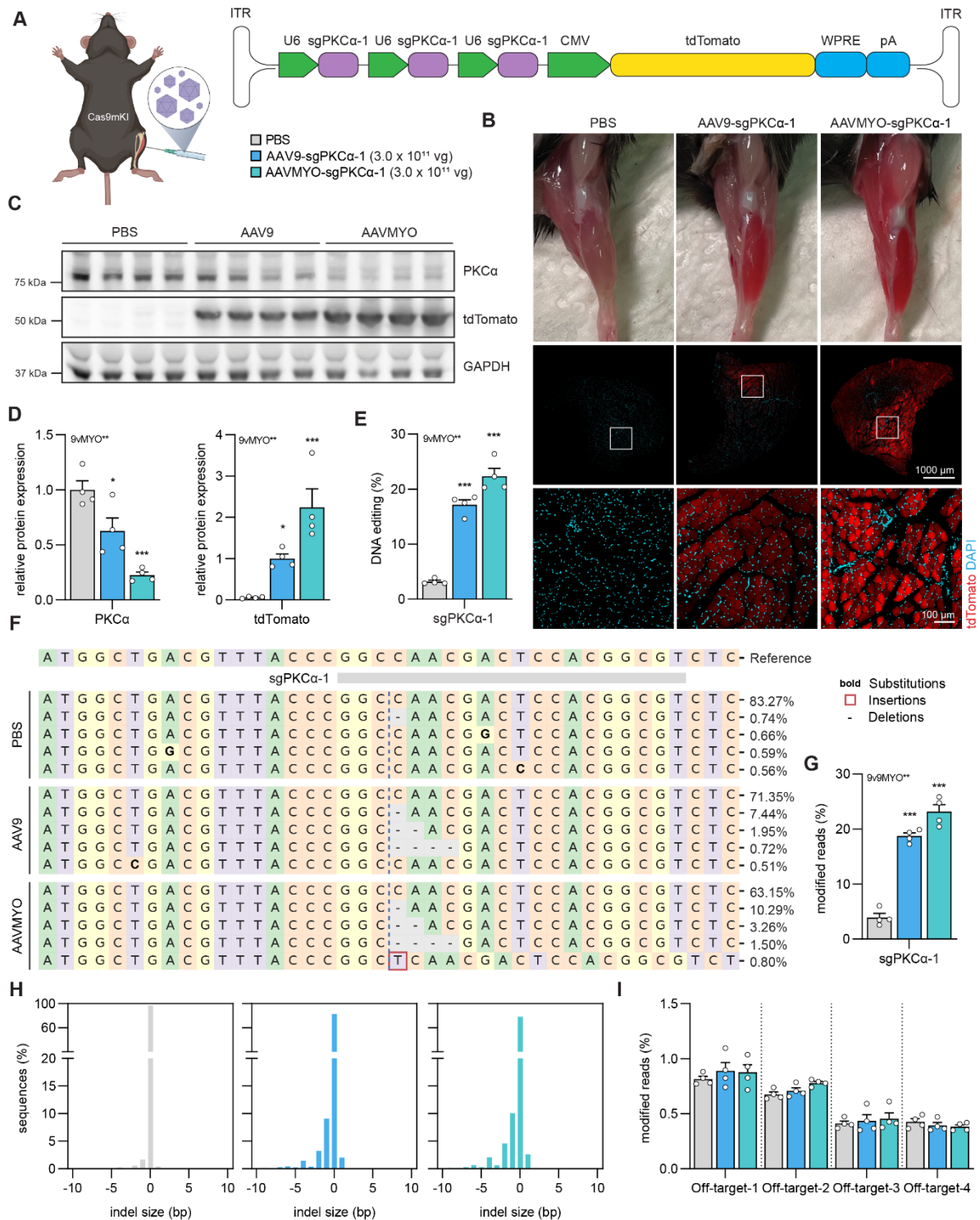
Figure 3: AAVMYO-mediated sgPKCα-1 delivery into TA muscle results in strong reduction of PKCα.

(A) Schematic presentation of the experimental procedure. For abbreviations, see legend to Figure 2. (B) Representative images of the injected hindlimb and of cross-sections of *tibialis anterior* (TA) muscle stained for tdTomato (red) and DAPI (blue), 6 weeks post-intramuscular injection of PBS or AAVs (3.0 x 10^11 vg) into Cas9mKI mice. (C) Western blot analysis and quantification (D) for PKCα and tdTomato in TA muscle lysates of Cas9mKI mice injected with PBS (grey), AAV9-sgPKCα-1 (light blue) or AAVMYO-sgPKCα-1 (cyan) 6 weeks post-injection. (E) Total INDEL formation analysis by TIDE. (F) Representative

34

704   sequence frequency table of reads using DNA isolated from TA under the different conditions covering

705   the sgPKCα-1 target region. (G) Relative number of modified reads under the different conditions in

706   the sgPKCα-1 target region. (H) INDEL size histogram indicating mutation distribution at the sgPKCα-1

707   target region in TA muscle of Cas9mKI mice. Conditions are injection of PBS (light grey, left), AAV9-

708   sgPKCα-1 (light blue, middle) or AAVMYO-sgPKCα-1 (cyan, right). (I) Total amount of mutated reads of

709   amplicons covering the top four predicted off-target loci in the different experimental paradigms.

710   There is no difference in the modified reads compared to PBS injection. Data are means ± SEM. N = 4

711   mice for each condition. Statistical significance is based on one-way ANOVA with Fishers LSD post-hoc

712   test. *P < 0.05, **P < 0.01, ***P < 0.001.
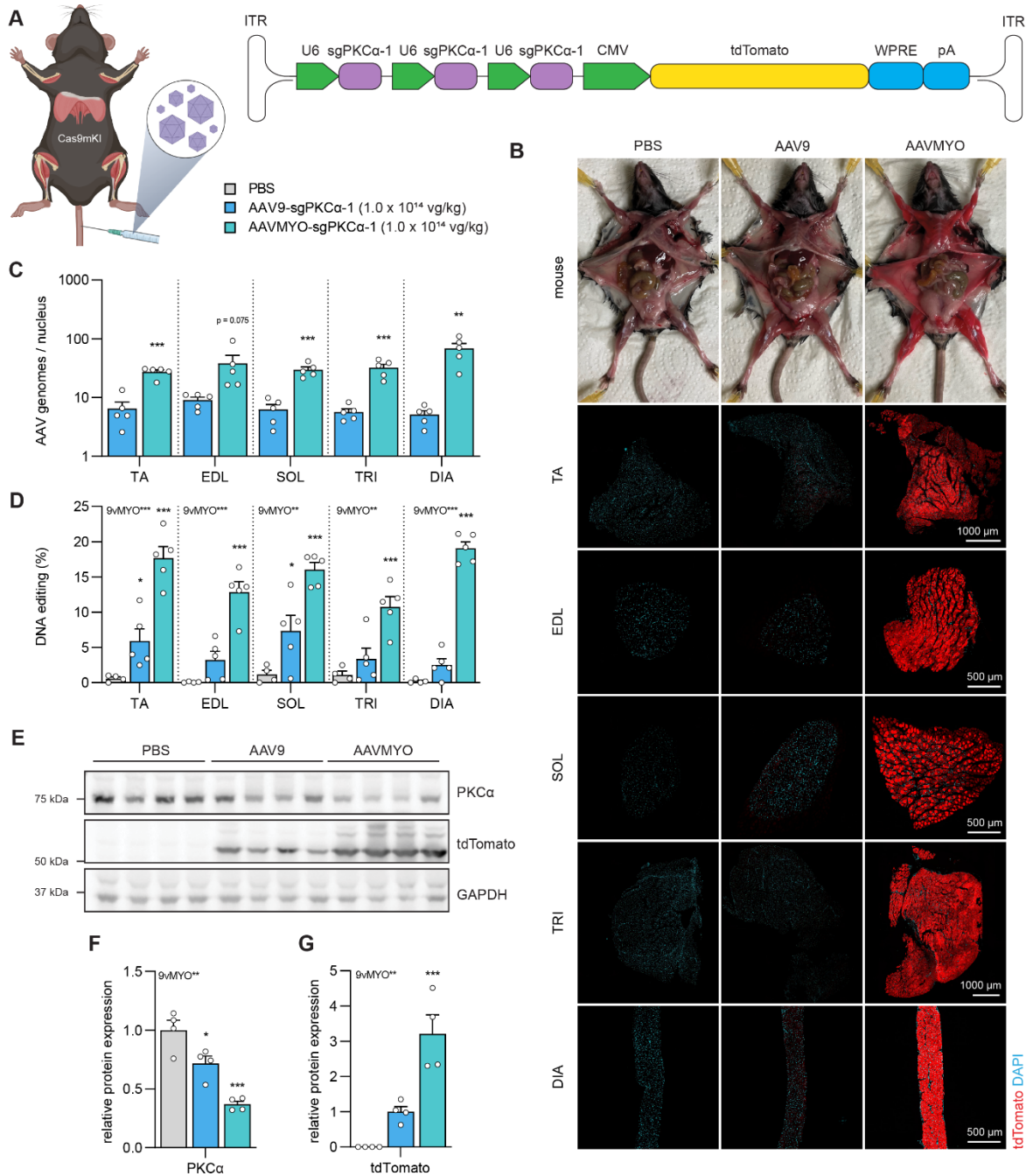
Figure 4: Systemic administration of AAVMYO-sgPKCα-1 *via* the tail vein into Cas9mKI mice reduces PKCα protein. (A) Schematic presentation of the experimental procedure. For abbreviations, see legend to Figure 2. (B) Representative images of dissected mice and cross-sections of *tibialis anterior* (TA), *extensor digitorum longus* (EDL), *soleus* (SOL), *triceps brachii* (TRI) or diaphragm (DIA) muscle stained for tdTomato (red) and DAPI (blue), 6 weeks post-intravenous injection of PBS or AAV (1.0 x 10^{14} vg/kg) into Cas9mKI mice. (C) Distribution of AAV in TA, EDL, SOL, TRI and DIA upon intravenous injection of AAV9-sgPKCα-1 (light blue) and AAVMYO-sgPKCα-1 (cyan) into Cas9mKI mice. (D) Total INDEL formation analysis by TIDE. (E) Western blot analysis and quantification (F, G) for PKCα (F) and tdTomato (G) in TA muscle of Cas9mKI mice injected with PBS (grey), AAV9-sgPKCα-1 (light blue) or

723   AAVMYO-sgPKCα-1 (cyan). Data are means ± SEM. N = 4 - 5 mice. Significance was determined using

724   one-way ANOVA with Fishers LSD post-hoc test (D, F, G) or unpaired t-test (C). *P < 0.05, **P < 0.01,

725   ***P < 0.001.
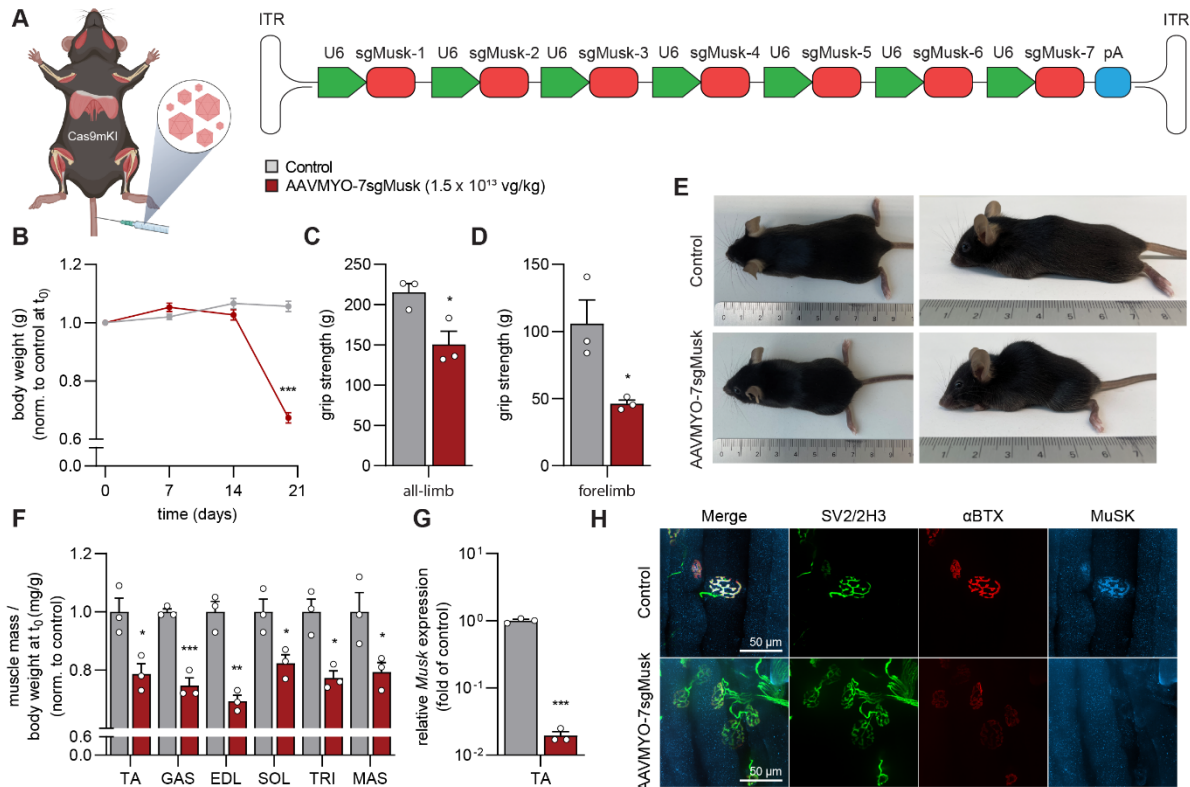
Figure 5: AAVMYO-CRISPR/Cas9 mediates systemic knockout of *Musk* and results in the loss of NMJs.

(A) Schematic presentation of the experimental procedure. (B) Body weight progression of controls (grey) and AAVMYO-7sgMusk-injected Cas9mKI mice (red). All-limb (C) and forelimb (D) grip strength of control and AAVMYO-7sgMusk-injected Cas9mKI mice, 20 days post injection. (E) Representative photograph of control and AAVMYO-7sgMusk-injected Cas9mKI mice, 20 days post-injection. (F) Changes in mass of TA, GAS, EDL, SOL, TRI and *masseter* (MAS) muscle of AAVMYO-7sgMusk-injected Cas9mKI mice, compared to controls. (G) Relative mRNA expression of *Musk* in AAVMYO-7sgMusk-injected TA muscle of Cas9mKI mice. (H) Representative images of whole-mount preparations of EDL muscles of controls and Cas9mKI mice injected with AAVMYO-7sgMusk. The presynaptic nerve terminals are stained with a mixture of antibodies directed against synaptic vesicle glycoprotein 2A (SV2; yellow) and neurofilament (2H3; green). Fluorescently-labeled α-bungarotoxin (αBTX; red) was used to visualize postsynaptic AChRs. MuSK protein was stained using a specific antibody (blue). Data are means ± SEM. N = 3 mice. Statistical significance is based on unpaired t-test comparing to control. *P < 0.05, **P < 0.01, ***P < 0.001.
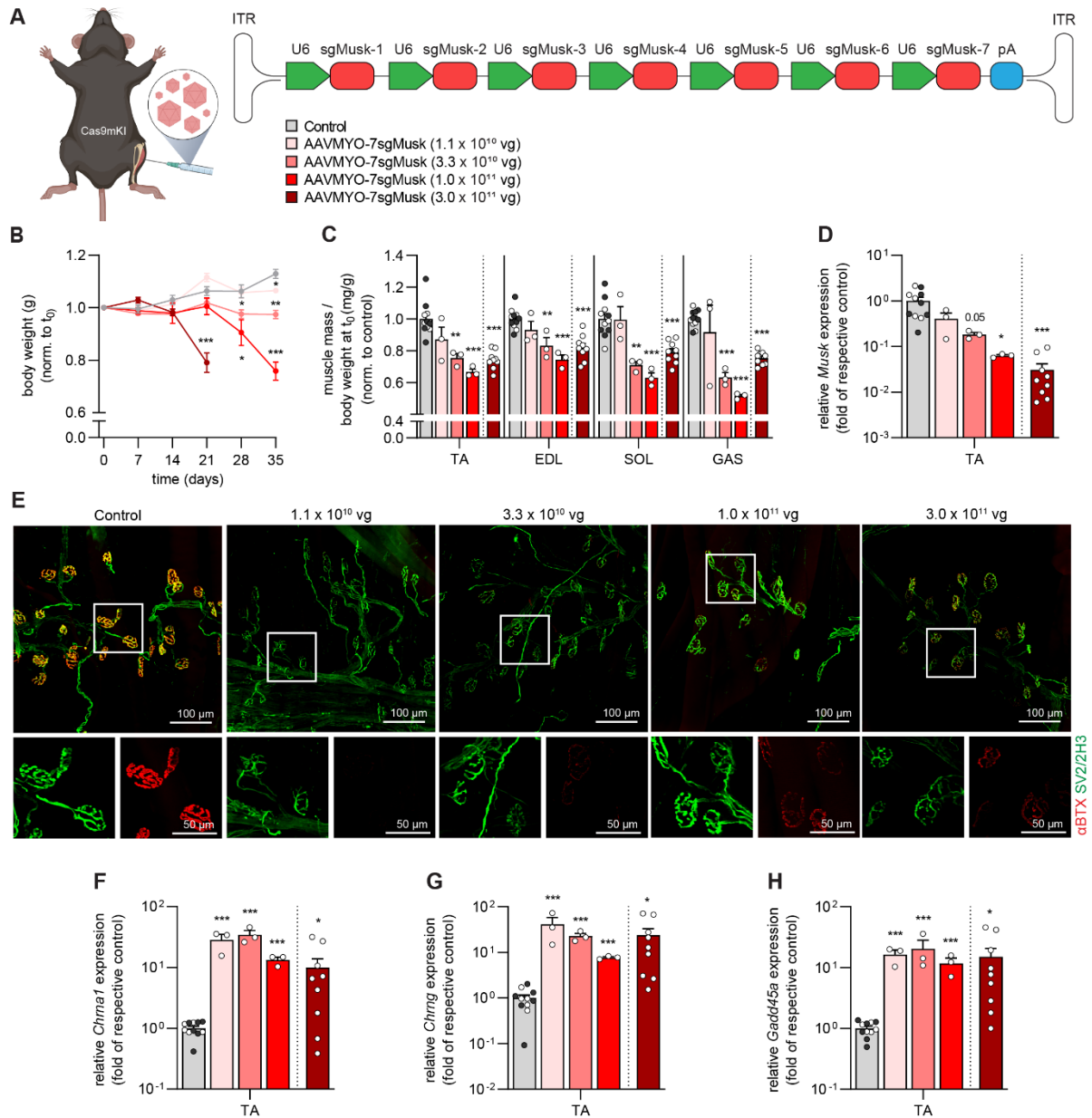
Figure 6: AAVMYO-CRISPR/Cas9 mediates local knockout of *Musk* and results in the loss of NMJs. (A) Schematic presentation of the experimental procedure using different amounts of sgRNA-delivering AAVMYO. (B) Body weight progression of controls (grey) and AAVMYO-7sgMusk-injected Cas9mKI mice (red colors) at the indicated doses. (C) Changes in muscle mass of AAVMYO-7sgMusk-injected Cas9mKI mice, compared to controls that included PBS-injected Cas9mKI mice (white dots) and AAVMYO-7sgMusk-injected wild-type mice (black dots). Values in the two control groups did not differ and were therefore combined. (D) Relative mRNA expression of *Musk* in AAVMYO-7sgMusk-injected TA muscle of Cas9mKI mice. (E) Representative whole-mount images of EDL muscles of controls and Cas9mKI mice injected with the indicated amount of AAVMYO-7sgMusk. The presynaptic nerve terminals are stained with a mixture of antibodies directed against synaptic vesicle glycoprotein 2A (SV2; yellow) and neurofilament (2H3; green). Fluorescently-labeled α-bungarotoxin (αBTX; red) was

753   used to visualize postsynaptic AChRs. (F – H) Relative mRNA expression of denervation marker genes

754   as indicated in AAVMYO-7sgMusk-injected TA muscles of Cas9mKI mice and controls. Note that

755   Cas9mKI mice injected with the highest AAVMYO-7sgMusk dose were analyzed at 3 weeks post-

756   injection while all the other mice were analyzed 5 weeks post-injection. Data are means ± SEM. N = 3-

757   11 mice. Statistical significance is based on unpaired t-test comparing to control. *$P < 0.05$, **$P < 0.01$,

758   ***$P < 0.001$.
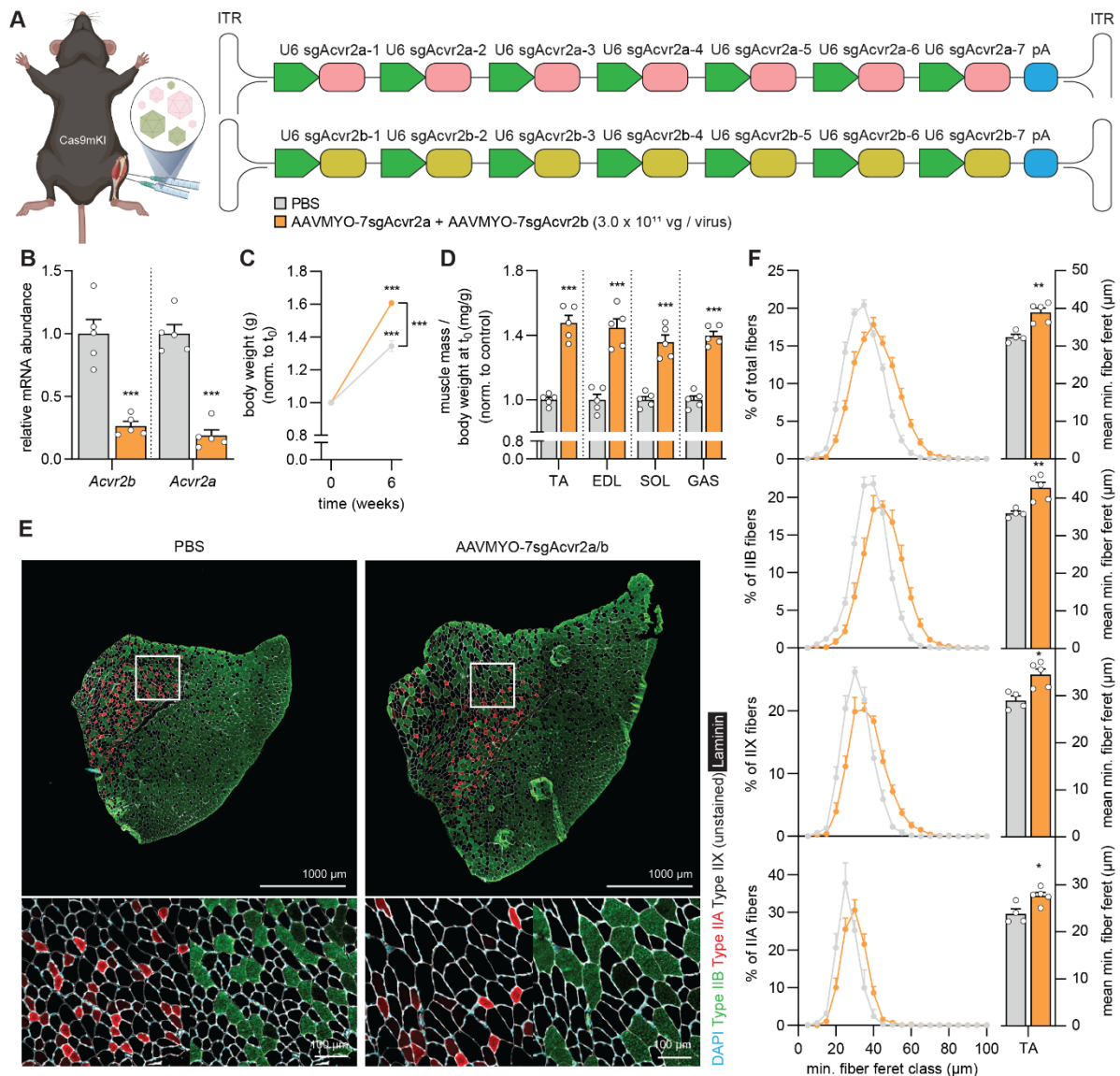
Figure 7: AAVMYO-CRISPR/Cas9-mediated double knockout of *Acvr2a/Acvr2b* causes strong skeletal muscle fiber hypertrophy. (A) Schematic representation of the experimental procedure. (B) Relative mRNA expression of *Acvr2a* and *Acvr2b* in *gastrocnemius* (GAS) muscle of Cas9mKI mice, injected with PBS or AAVMYO-7sgAcvr2a/b 6 weeks post-injection. (C) Body mass of Cas9mKI mice before and 6 weeks after intramuscular injection of PBS (grey) or AAVMYO-7sgAcvr2a/b (orange). (D) Mass of *tibialis anterior* (TA), *extensor digitorum longus* (EDL), *soleus* (SOL) and GAS muscles of the AAVMYO-7sgAcvr2a/b-injected (orange) or PBS-injected (grey) legs of Cas9mKI mice. (E) Representative images of TA cross-sections stained with antibodies to type IIB (green), type IIA (red), laminin (white) and with DAPI (blue) from Cas9mKI mice injected as indicated. Note that type2X muscle fibers are not stained. (F) Total and fiber type-specific minimal fiber feret distribution (left) and mean minimal fiber feret (right) of TA muscle of Cas9mKI mice, injected with PBS (grey) or AAVMYO-7sgAcvr2a/b (orange). Data are means ± SEM. N = 4-5 mice. Statistical significance is based on unpaired t-test. *$P < 0.05$, **$P < 0.01$, ***$P < 0.001$.